Chapter 10

Atomic Force Microscopy of Isolated Mitochondria

Bradley E. Layton and M. Brent Boyd

Abstract

This chapter describes methods for isolating and imaging metabolically and toxicologically challenged mitochondria with atomic force microscopy. Mitochondria were isolated from rat dorsal root ganglia or brain and exposed to glucose or dinitrobenzene (DNB) to simulate the cellular environment of a diabetic animal that has been exposed to excess glucose or to DNB. It is one of only a few articles to present images of membrane structures, such as voltage-dependent, anion-selective channel pores, on intact organelles. The purpose of the chapter is not to report on the metabolic or toxic effects, but to communicate in more detail than a typical journal paper allows the methods used to image isolated organelles. We also provide a series images revealing the outer membrane and outer membrane pores. An image of an isolated nucleus as well as a set of notes written to avoid common pitfalls in isolation, labeling, and imaging is also included.

Key words: AFM, Mitochondria, VDAC, Organelle, In situ, Membrane imaging, Apoptosis

1. Introduction

In the original work (1) that provided the impetus for this chapter, we explored the hypothesis that in the presence of excess glucose, one or more mitochondrial membrane proteins may become altered, in either morphology or prevalence, leading to a metabolic cascade causing the production of oxidizing agents that eventually destroy mitochondria and subsequently the neurons they support. For review, see ref. 2. A primary challenge in the preparation and subsequent atomic force microscopy (AFM) imaging of single mitochondria was to determine their optimal concentration after isolation from both embryonic rat dorsal root ganglia (DRG) and SY5Y cells. Fluorescence imaging was performed prior to AFM after using a mitochondria isolation

Pier Carlo Braga and Davide Ricci (eds.), *Atomic Force Microscopy in Biomedical Research: Methods and Protocols*, Methods in Molecular Biology, vol. 736, DOI 10.1007/978-1-61779-105-5_10,

technique derived from ref. 3. This chapter outlines in detail isolation methods, imaging techniques, and provides suggestions for streamlining the process.

The research challenge and primary contribution were to establish whether or not mitochondrial membrane proteins and the outer membrane itself become altered in situ as quantified by morphological features at the surface of glucose-challenged or dinitrobenzene (DNB)-challenged mitochondria. Imaging membrane-bound proteins and other membrane morphological features in whole, isolated mitochondria had not been accomplished prior to our work. In addition to a description of the imaging techniques, we provide example images obtained from the technique developed.

The atomic force microscope is an ideal tool for imaging in situ proteins, and our investigation was one of the first to attempt to observe proteins in intact organelles. Other AFM-based approaches include the imaging of mitochondria with immunogold labeling (4), isolated outer mitochondrial membranes with intact voltage-dependent, anion-selective channel (VDAC) pores (5, 6), isolated nuclear membranes (7), and imaging single cells, such as spermatozoa (8) or neurons (9). AFM has also been used to perturb whole cells in an effort to track the resulting movement of groups of mitochondria near the point of tip contact (10). With its subnanometer resolution, and the ability to image in aqueous environments, it is also well suited to image organelle membrane proteins in situ (4) or in monolayers (11–14). In this regard, AFM is thus frequently used as a complementary technique to SEM and is often invaluable for imaging subcellular structures since less sample preparation is generally needed, and sputtering artifacts are eliminated (15). However, two other relevant papers (16, 17) obtained images of membrane proteins in air contact mode (see Note 1).

There has been a relatively recent revolution in the description of the morphology of the mitochondrial inner membrane. The textbook "radiator-fin" shape presented decades ago is no longer valid. Recent three-dimensional reconstruction techniques of thick-sectioned TEM preparations of single mitochondria have revealed that the cristae form tubular structures 30–40 nm in diameter and several hundred nanometers in length (18). Other evidence indicates that under altered chemical environments, mitochondria themselves may become dramatically reticulated (19).

There is strong evidence that mitochondrial size increases in the presence of excessive glucose. This was found by Russell et al. (20), where mitochondria from rat primary DRGs challenged with 45 mM glucose for 6 h sustained an increase in

cross-sectional area of ~50% ($0.43 \pm 0.03\ \mu m^2$ vs. $0.66 \pm 0.08\ \mu m^2$). This increase in size was also found to be dose- and time-dependent, with increased glucose molarities resulting in greater swelling rates, and longer exposure resulting in greater size increases. A plateau appears to be reached somewhere between 24 and 48 h of excessive glucose exposure. This time course appears to coincide with the complete membrane depolarization at 24 h.

In addition to being key components in metabolic disorders, mitochondria may also play an important role in infectious disease pathways. For example in hepatitis, the presence of the hepatitis B protein HBx has been implicated in the opening of the so-called mitochondrial permeability transition pore (21–23). One of the most thoroughly studied mitochondrial proteins is VDAC (24), so named because it is selectively permeable to anions. Expressed in the nucleus, but found in the outer membranes of mitochondria, its molecular mass is ~30 kDa and occurs at a mean density of 10^3–10^4 per μm^2 on the outer membrane surface (25). Approximating a single mitochondrion as a sphere with a radius of 0.25 μm yields an approximate mitochondrial surface area of $4\pi r^2 = 0.8\ \mu m^2$, and thus between 800 and 8,000 VDAC pores per mitochondrion. The VDAC diameter reported by Manella (25) is 4.3–5.3 nm with an inner pore diameter of 2–4 nm, and a 0.5 nm projection from the outer membrane surface. A general three-dimensional shape of the VDAC pore has also been obtained by electron crystallography (25), confirming pore geometry. The functional implications of this is that VDAC is easily permeable to many respiration-related and metabolism-related molecules, such as AMP, ADP, ATP, inorganic phosphate, acylcarnitine (26), or other molecules, with diameters <1 nm (27). Thus, the ability to quantify number, spatial distribution, and potentially the state of individual porins may yield valuable insight into the molecular mechanisms of apoptosis. Despite the progress made in imaging isolated mitochondria and isolated mitochondrial membrane proteins, however, the direct observation of a dynamic pore formation event is yet to be achieved. It is commonly thought to be comprised of VDAC, adenine nucleotide translocase (ANT), and cyclophilin D. However, VDAC and ANT can be deleted and the mitochondrial permeability transition still occurs implying that may facilitate pore formation, but are not necessarily required for it to occur. Some investigators believe that its opening is required to release calcium, whereas others argue that a closed pore actually releases more calcium from the mitochondria. Additionally, some claim that a closed MPTP facilitates apoptosis whereas others argue that an open MPTP facilitates apoptosis. Thus, there is likely a prominent role to play for AFM in preparations of living and metabolically active mitochondria. For further reading see ref. 28.

2. Materials

2.1. Chemicals

1. Sodium pentobarbital (100 mg/kg) for rat euthanization.
2. Trypsin (0.25 M) for cell dissociation.
3. Ice-cold isotonic (pH = 7.4) phosphate-buffered saline for suspension of cells subsequent to DRG removal.
4. Protease inhibitor, such as leupeptin, aprotinin, or phenylmethanesulphonylfluoride (PMSF), for arresting trypsin activity.
5. Glucose or other metabolite for providing a metabolic challenge to mitochondria.
6. Mannitol for use as a glucose control.
7. Paraformaldehyde (4%) for mitochondria fixation.
8. DNB for mitochondrial toxicity challenge.

2.2. Atomic Force Microscopy

1. Digital Instruments Bioscope AFM model BS3-N2 with a Nikon eclipse TE2000-U optical microscope, using Nanoscope Software v 5.12r5 also from Digital Instruments (Santa Barbara, CA).
2. AFM tips. These may be either tapping or contact with spring constants $k = 0.1–1.0$ N/m, or natural frequencies of $\omega_n \sim 300$ kHz (air) or ~10 kHz (fluid). For these experiments, the "short skinny" tips DNP-S (sharp, silicon nitride probes, Veeco Probes), were used.
3. Poly-L-lysine glass slides, e.g., (Polysciences 22247-1 or poly-L-lysine Biocoat® from six-well plastic plates from Becton–Dickinson, 354413 or BD two-well poly-L-lysine slides, 354629) for making mitochondria adherent to imaging substrate.

2.3. Animals, Cells, and Organelles

1. Adult female Sprague-Dawley rats.
2. We used mitochondrial samples extracted from embryonic rat DRG, adult rat liver, and from SY5Y cells, an immortalized neural cell line originally expanded from a bone tumor in 1970. The SY5Y cells were obtained for the purpose of isolation procedure verification, since extraction from embryonic DRG mitochondria is more challenging and expensive.
3. Three groups of embryonic rat DRG mitochondria samples were assigned notation (Table 1).

Table 1
Embryonic rat DRG, rat liver, and SY5Y mitochondria samples collected on 4-28-03, 5-06-03, and 5-20-03 as well as for rat liver mitochondria from previous successful imaging

Sample	Notation
Neural control	C
Neural mannitol	M
Neural glucose	G_n
SY5Y	SY5Y
Liver control unfixed	N
Liver control fixed	N_f
Liver glucose unfixed	G
Liver glucose fixed	G_f
Liver DNB-challenged	DNB

3. Methods

3.1. Isolation

1. Using the National Research Council's "Guide for the Care and Use of Laboratory Animals," one E15 rat, with 17 embryos, was euthanized using sodium pentobarbital (100 mg/kg) injected intraperitoneally. Dissection begins once no involuntary response results from a strong pinch to the paw pads. Other euthanization techniques, such as decapitation or asphyxiation, are thought to produce rapid alterations in the metabolic state of the animal and may lead to altered mitochondrial states. From each embryo, as many DRGs as possible were extracted under a dissecting microscope with Roboz 0.20 mm × 0.12 mm tweezers. In this case, approximately 500 DRG clusters were extracted in approximately 2 h. Extraction of mitochondria from liver cells is identical with the exception that the liver tissue must be dissected and homogenized cold prior to trypsinization. SY5Y cell prep is identical to that of both DRG and liver from this point forward. For a more in-depth description of dissection procedure, see Note 2 (29).
2. Cell clusters were then exposed to ice-cold trypsin (0.25 M) in phosphate-buffered saline for 10 min.

3. Suspension was then spun for 5 min at 2,200 × *g* in 1.8-mL tubes.
4. The pellet, which contained noncellular membrane material, was resuspended in 1 mL ice-cold isotonic buffer with a protease inhibitor, such as leupeptin, aprotinin, or PMSF.
5. Solution was then homogenized with a glass Dounce homogenizer, e.g., MS851 Acris Antibodies (Germany) on ice for 20 strokes to further gently disrupt cell membranes.
6. Subsequent to homogenization, 1 mL ice-cold isotonic buffer and protease inhibitor were added to arrest damage to exposed mitochondria.
7. Solution was then spun at 900 × *g* for 5 min at −4°C in 1.8-mL tubes.
8. A 1-μL pellet of cells, nuclei, and other matter was removed using a 10-μL pipette. Note: for AFM, 1 μL is an enormous sample. The volume of a single mitochondrion is approximately 100 aL (100 attoliters = 10^{-16} L). Thus, a 1-μL sample could contain as many as ten billion mitochondria.
9. Supernatant containing mitochondria was carefully transferred into an ultracentrifuge tube with a 1-μL pipettor. Care was taken to not remove the uppermost layer of the supernatant in order to avoid lipid debris. The lower most layer was also avoided.
10. Solution was then spun at ~12,000 × *g* for 8 min in 1.8-mL tubes.
11. A small visible pellet with a footprint of less than a square millimeter is now resolvable. This pellet contains intact mitochondria.
12. Supernatant is then poured off or pipetted off and the pellet resuspended in 1 mL ice-cold isotonic buffer without protease inhibitors.
13. Respin solution at 12,000 × *g* for 8 min.
14. Pull off supernatant and resuspend pellet in 10 μL of ice-cold isotonic buffer. This step is critical for maintaining a high concentration of mitochondria. Resuspending in 100 μL results in a concentration that is too sparse for AFM imaging. Using a volume smaller than 10 μL, if feasible, may be desirable if the pipettor is skilled and the sample can be kept hydrated prior to and during imaging.

3.2. Treatment

1. At this point glucose, mannitol or DNB challenge may be added. In the present study, treatments were started midday after dissections were complete, and metabolic or toxic challenge was added to suspensions at 4°C on agitator for approximately 2 h. Care must be taken to avoid sample from interacting with the container lid to avoid mitochondria

coming out of solution. Samples may be directly imaged or stored at 4°C overnight.

2. At this point, prior to storage, 2–4% paraformaldehyde may be added to fix cells prior to AFM imaging.

3.3. Atomic Force Microscopy

1. Pipette cells onto polylysine slides and keep them moist if fluid-tapping mode is desired. The time required to align the AFM laser and position the sample under the tip is typically sufficient to allow the mitochondria to become adherent. This occurs through surface charge reactions (Fig. 1). A typical view of the mitochondria or mitochondrial clusters looks similar to the image seen in Fig. 2. At this point in the process, patience must be practiced. Obtaining a few quality AFM images can take a full day in the lab, and obtaining them consistently can take weeks or months of practice. In placing the tip near the target, begin with the "best guess" as to where the tip is actually located on the cantilever and aim directly for the sample (see Note 2) (see Fig. 3). Distinguishing stationary from suspended particles is best accomplished by creating

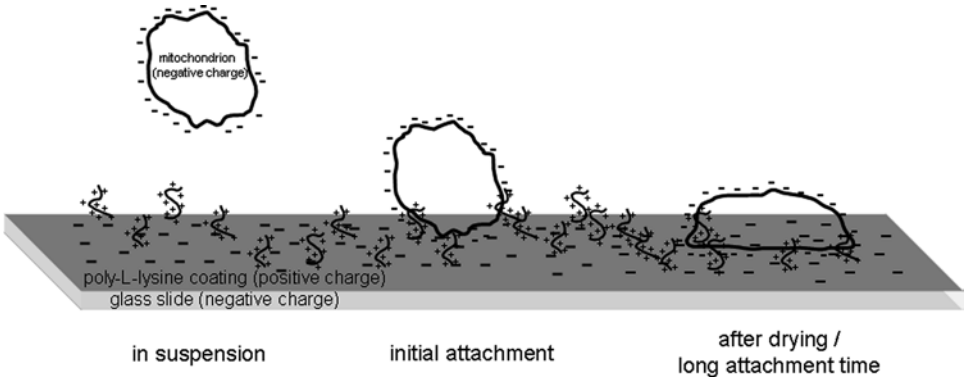

Fig. 1. After attaching to poly-L-lysine-coated slide, mitochondria are likely to flatten as increasing numbers of adhesion sites become bound to the lysine. Additionally, if samples are allowed to dry as is necessary for air contact mode atomic force microscopy, mitochondrial volume is likely to decrease due to water loss from the matrix.

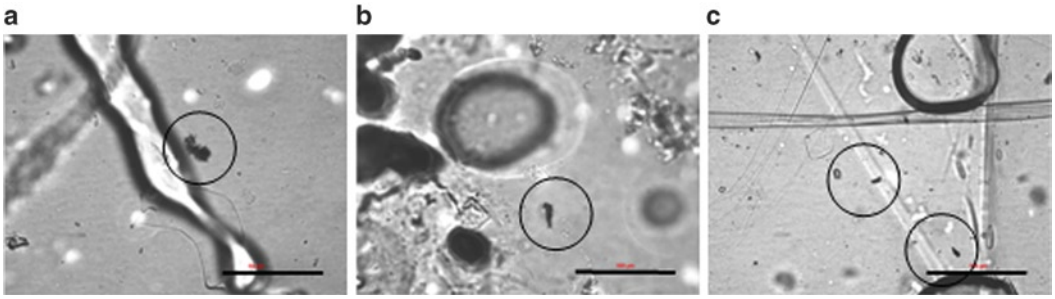

Fig. 2. Light microscopy Images of clusters of isolated mitochondria on mica at 400×. (**a**) control (**b**) mannitol-control, (**c**) glucose-challenged. Scale bars = 100 μm (see Note 4).

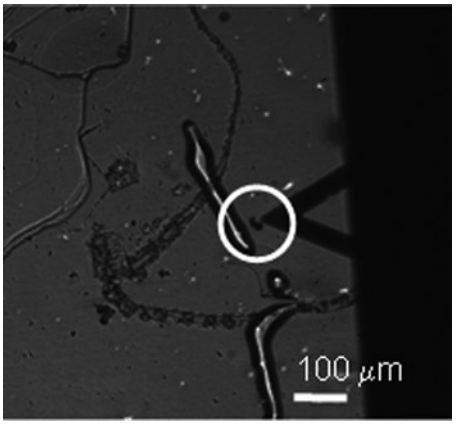

Fig. 3. AFM tip being brought into proximity of the apparent cluster of control mitochondria. Scale bar = 100 μm.

small waves with a pipette while searching for imageable clusters. Clusters that are not moving as a result of wave motion are likely stuck to the lysine and are the best candidates for imaging. Ideally, a rinse should be done at least once to remove unattached debris from the imaging field that might interfere with the laser or cantilever. It is typically good practice to allow the microscope to complete a 1 μm × 1 μm scan before attempting to fine tune gain, target force, scan size, and scan rate settings (see Note 3). Gradually begin increasing scan size until sample becomes visible, then begin optimizing settings for minimal force by moving the deflection set point away from 0 V and toward –2 V until image disappears, and then return to surface by slowing moving back toward 0 V until image reappears. In tapping mode, begin moving amplitude set point toward the free amplitude until image disappears, then gradually bring amplitude set point back until image reappears. Typical TMR values should be ~1 nm, once tip force was minimized. All imaging for this work was performed at an RMS amplitude of approximately 1 V.

2. Alternatively, if the AFM is equipped with fluorescence imaging, individual mitochondria or mitochondrial clusters may be labeled with MitoTracker® (e.g., Invitrogen formerly M7514 Molecular Probes) and applied according to the manufacturer's specifications, typically at a concentration of 1–10 nM (Fig. 4). MitoTracker green is excited at 490 nm and emits at 516 nm. Images were taken with a Nikon Microphot microscope and captured on a SPOT RT digital camera.
3. In our original study, fluorescence was not available on the AFM optical microscope and we relied on a probabilistic

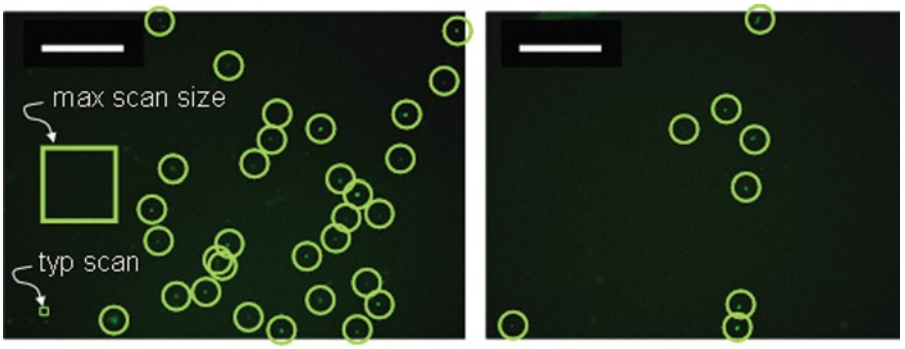

Fig. 4. Fluorescence imaging of mitochondrial preparations reveals that the mitochondrial yield is approximately 150 clusters per mm^2 in a 1-μL sample on the left, and fewer than thirty in a 10 μL sample on the right. A maximum AFM scan and a typical AFM scan (10 μm × 10 μm) is shown for comparison in the left image. Scale bars = 100 μm.

formula for finding individual mitochondria. For example, with random placement of the tip in a sparse population of mitochondria and 10 μm × 10 μm scans, each of which takes approximately 10 min to acquire, the probability of success is approximately 5–10% after an hour and a half of imaging.

4. If imaging cannot occur immediately after dissection and dissociation, fixation and storage may be used. In this study, several mitochondria were imageable after nearly a year in storage at 4°C. To do so, respin for 5 min at 12,000 × *g*, remove supernatant, and resuspend pellet in 1–10 μL of 10–100 nM MitoTracker Green. Gently spin and resuspend, and pull off 1 μL for fluorescence imaging as above. Another alternative is to add an anti-fade reagent (e.g., ProLong® Invitrogen).

After a 20 μm × 10 μm scan, a typical cluster may appear as in Fig. 5.

Heights of some of the mitochondria were as large as 500 nm trailing down to less than 50 nm. Several spherical-like structures with diameters on the order of 0.5 μm were found in all three of the samples G, M, and C, indicating that mitochondria were in fact present in these preparations as evidenced in the fluorescence imaging (G shown in Fig. 6). Under a coverslip, the entire 1 μL droplet spreads to a diameter of approximately 1 cm (~80 mm^2), yielding a volumetric density of approximately 10^6 mitochondria (or clusters) per microliter. Using an order-of-magnitude calculation, with an approximate mitochondrial radius of 0.5 μm and approximating a mitochondrion as a sphere, a typical mitochondrion volume is

$$V_{\mathrm{Mt}} = \frac{4}{3}\pi r_{\mathrm{Mt}}^3 = \frac{4}{3}3.14(0.25\mu\mathrm{m})^3 = 0.065\mu\mathrm{m}^3 = 65\,\mathrm{aL}.$$

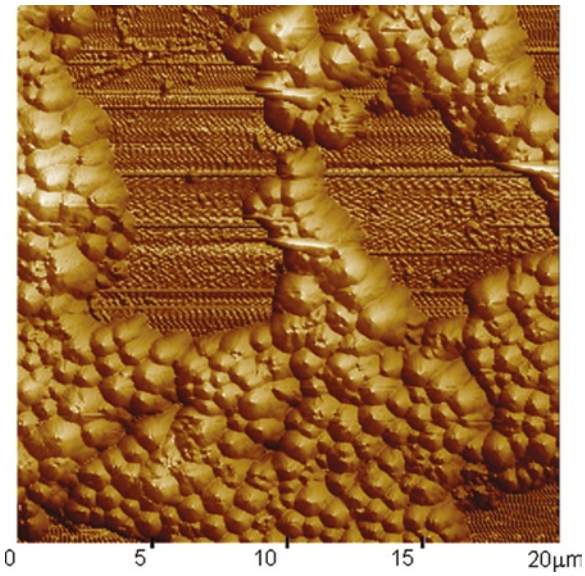

Fig. 5. (**a**) Two-dimensional images of SY5Y mitochondria imaged in air contact mode. Scale = 20 μm.

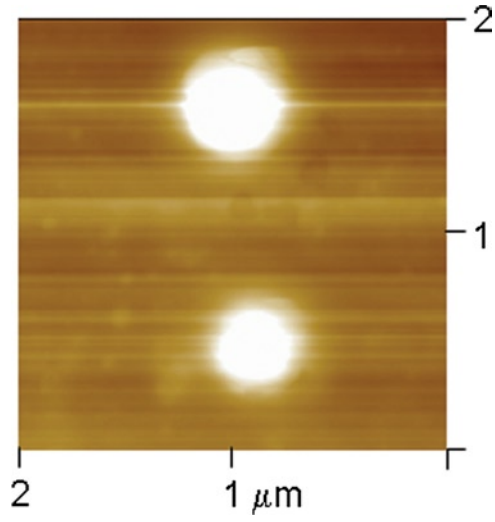

Fig. 6. 2 μm × 2 μm scans of glucose-challenged mitochondria imaged in air-contact atomic force microscopy.

3.4. Fortuitous Impurities

After several instances where apparent mitochondrial clusters stuck to the tip upon attempting to engage, a series of images were obtained of an apparent mitochondrial cluster. As mentioned previously, the method that appeared to be most successful was that of lowering the tip directly onto the sample as opposed to approaching it laterally, thus reducing the chance of releasing it from the poly-L-lysine substrate. The cluster appeared to be only

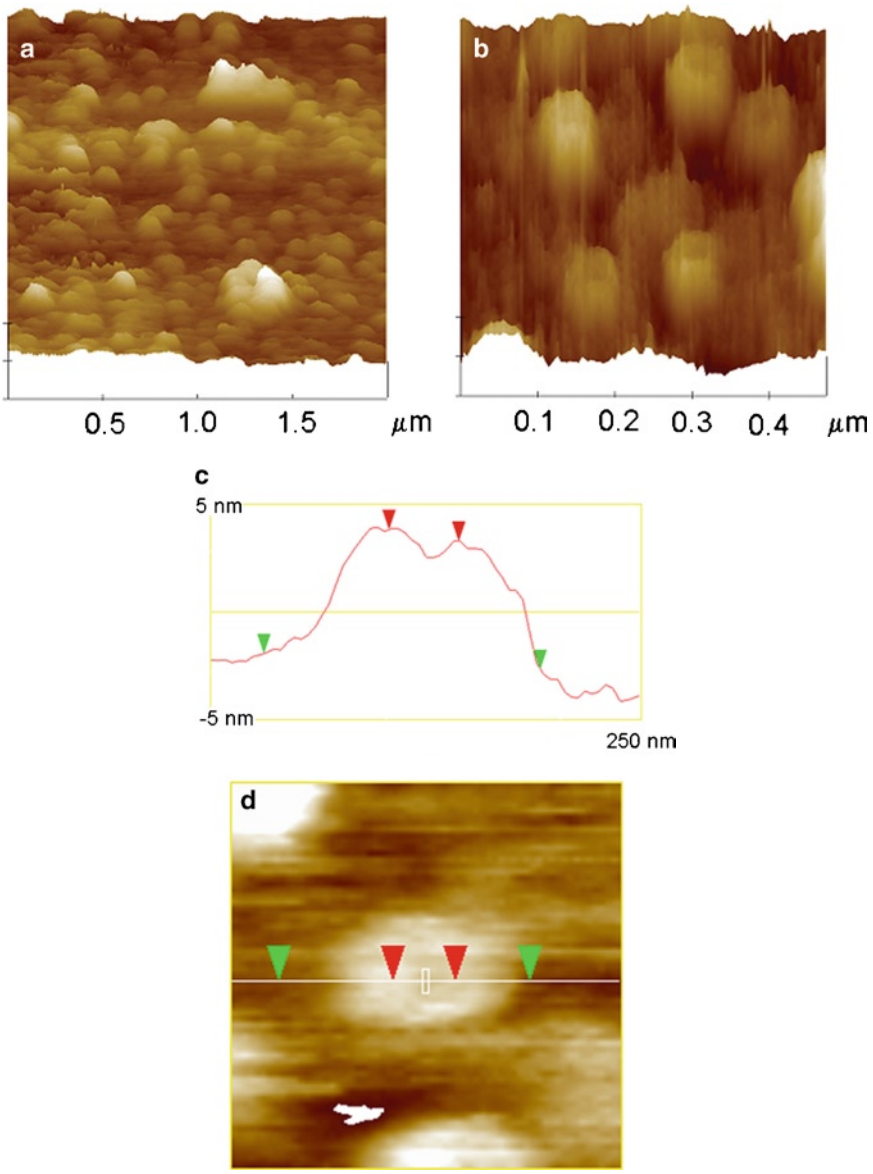

Fig. 7. Fluid-tapping atomic force microscopy image of 3hr-glucose challenged unfixed mitochondria preparation from embryonic rat DRGs. (**a**) 2 μm × 2 μm Scan of apparent nuclear (**b**) 250 nm close-up of region. (**c**) Cross-sectional analysis and (**d**) top projection of apparent pore showing pore diameter of ~10 nm. As an alternative, we could write *Red* (inner arrowheads) horizontal distance = 40 nm, *green* (outer arrowheads) horizontal distance = 158 nm.

loosely attached, however, since rescanning the same area often yielded a different image from the previous one. Most notable in these scans are the presence of structures with an approximate density of 50 per μm^2 (Fig. 7a) diameters of 100 nm (Fig. 7b) and an approximate height of 10 nm (Fig. 7c), and an apparent inner pore diameter of 10 nm (Fig. 7c and d). See Note 5.

The structures seen in Fig. 7 are almost certainly proteinaceous membrane pores. Upon attempting to obtain a larger scan size of the regions surrounding those seen in Fig. 7, to determine if the AFM tip was in fact on the cluster under it, or imaging something stuck to the lysine substrate, the cluster broke free and became unimageable. There exists the possibility that the image in Fig. 7 is the inner or outer surface of an outer mitochondrial membrane stuck to the lysine. Such a large (2 μm × 2 μm) region of membrane could be that of a single mitochondrion, since those shown in Fig. 7 are that of unfixed, glucose-challenged. There also exists the possibility that this is a fragment of nuclear membrane. As a very rough estimate of the molecular mass, M_o, of the protein being imaged, the following equation may be used:

$$M_o = \frac{N_A}{V_1 + dV_2} V_{prot},$$

where N_A is the Avogadro constant (6.022×10^{23} mol^{-1}), V_1 is the partial specific volume of the protein (0.74 cm^3/g), V_2 is the specific volume of water (1 cm^3/g), and d is a factor describing the extent of hydration. Shillers et al. (30) used d=(0.4 mol H_2O/mol protein) for their air-dried method. Substituting in values for our membrane protein with its height of ~4 nm, and d=1 for fluid, we obtain a molecular mass of ~10 kDa. Note that the protein radius of ~50 nm is likely to be overestimated by as much as 20% since its radius is approximately 10 nm (31). This protein size, however, is greater than that of the VDAC membrane protein reported in the literature (25).

3.5. Single Mitochondria at Close Range

The following sections (Figs. 8–13) consist of a series of images taken at scan sizes of approximately 500 nm × 500 nm of a single mitochondrion. Common to most is the indication that the inner membranous structure is partially visible, since it likely supports the outer membrane as the tip passes over.

3.6. Future Work

Future work may include attempting a membrane protein imaging method similar to that used by Schillers et al. (17) who obtained excellent results of protein density from frog oocyte membranes. The technical difficulties involved in "rolling out" a mitochondrial membrane onto a lysine slide may be much greater, since the frog oocyte is in fact macroscopic (~1 mm diameter) as compared to the <1 μm mitochondrial diameter. Another protein that may be imageable with the protocol described herein is the nuclear pore complex, or other nuclear membrane protein. In fact, a nucleus was imaged with the protocol described herein. The resulting image is shown elsewhere (32).

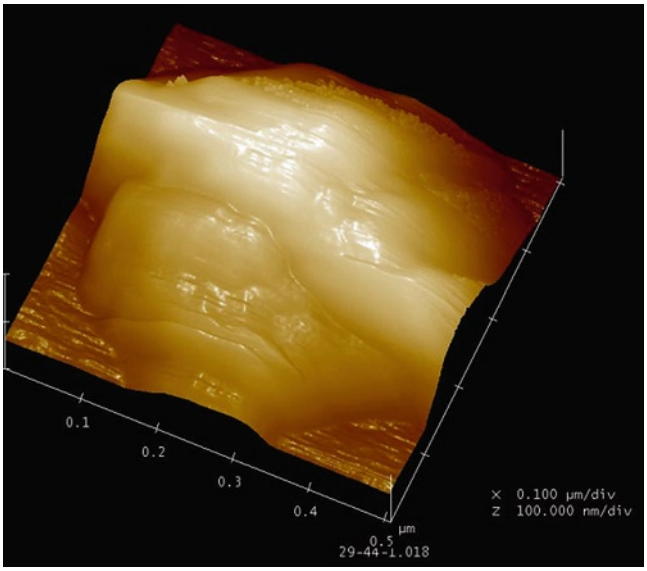

Fig. 8. Fluid-tapping atomic force microscopy image of unfixed control mitochondria from embryonic rat DRGs. Ridge seen running horizontally across image may be a result of this mitochondrion changing shape during imaging.

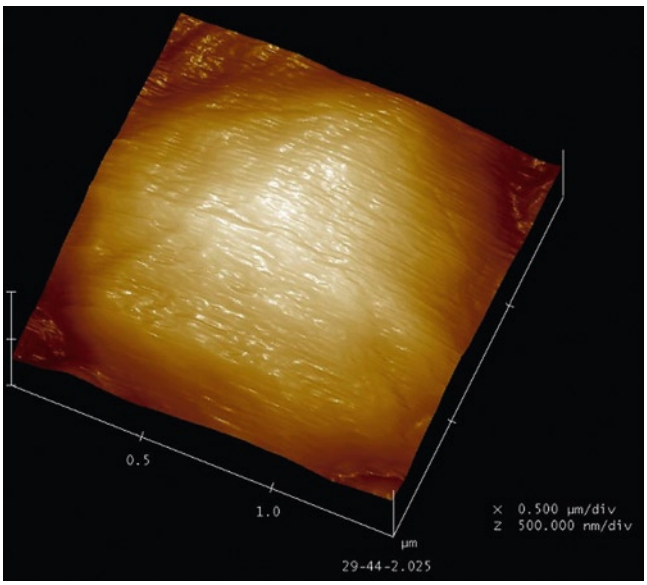

Fig. 9. Fluid-tapping atomic force microscopy image of fixed control mitochondria from embryonic rat DRGs. Overall morphology is more stable than seen in the unfixed specimens.

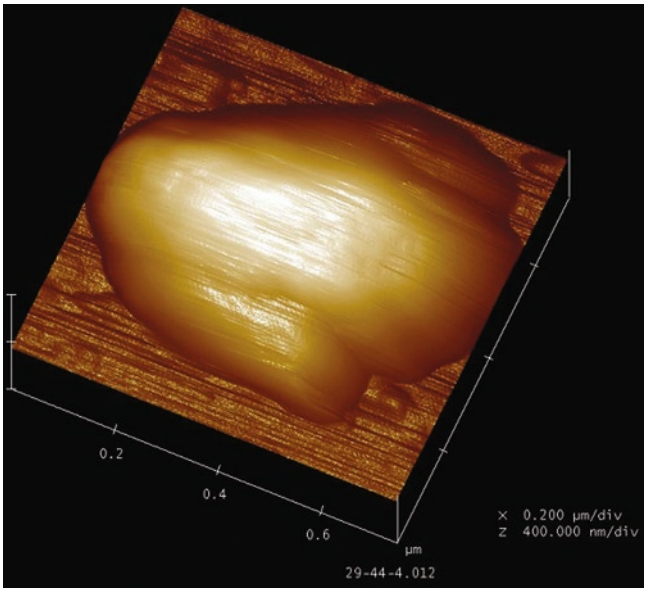

Fig. 10. Fluid-tapping atomic force microscopy image of fixed control mitochondria from embryonic rat DRGs. Overall morphology is more stable than seen in the unfixed specimens.

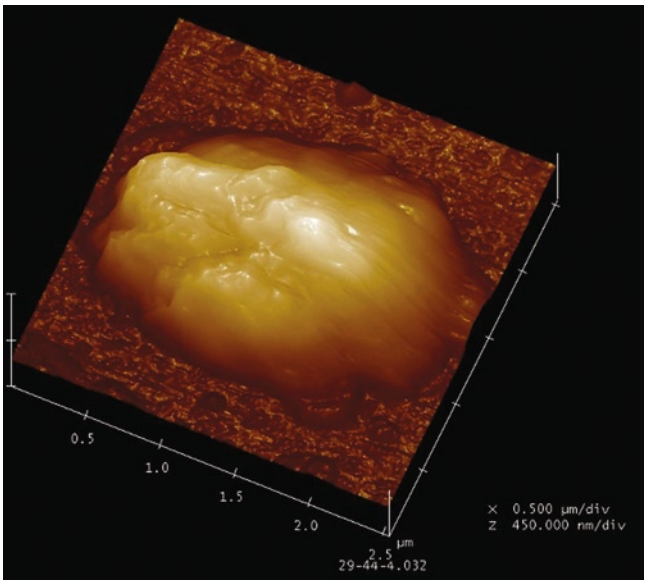

Fig. 11. Fluid-tapping atomic force microscopy image of fixed control mitochondria from embryonic rat DRGs. While more convoluted, than those seen above, overall morphology is more stable than seen in the unfixed specimens.

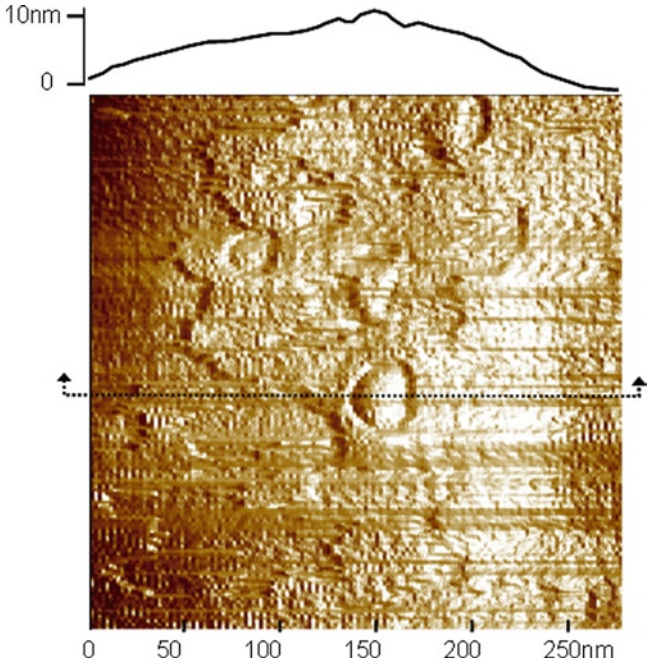

Fig. 12. Fluid-tapping atomic force microscopy image of fixed control mitochondria from embryonic rat DRGs depicting what appears to be a breach in the outer membrane. Whether caused by glucose challenge or sample preparation is yet unknown.

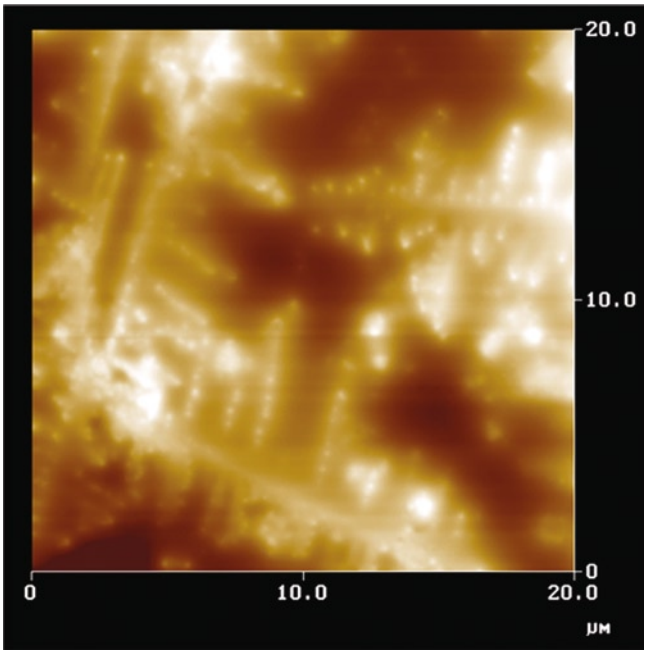

Fig. 13. 20 μm Scan of control DRG mitochondrial preparation in air contact mode atomic force microscopy showing crystalline structures presumably from dried salts in isotonic buffer. It is unclear whether or not the punctuating circular features along crystalline lines are mitochondria or not. Including only the circular features with diameters 0.5 mm or larger, results in ~10 in this 20 μm × 20 μm scan, or the equivalent of 250 per 100 μm × 100 μm area, 2.5× more than was seen with fluorescence imaging of the same sample preparation.

4. Notes

1. Two of the most relevant papers for this research, (16, 17), imaged in air. For example, Boujrad et al. (16) obtained AFM images of apparent clusters of an 18 kDa mitochondrial membrane protein, peripheral-type benzodiazepine receptor PBR, associated with the VDAC. Schillers et al. (14) obtained AFM images of at least two membrane proteins of *Xenopus laevis* oocytes. The heights of these membrane proteins were 10 and 14 nm, corresponding to molecular weights of 275 and 750 kDa, respectively.
2. Currently, the two most time consuming portions of the protocol are DRG removal and mitochondrial location. A large advantage would be gained if the location mitochondria could be visually verified immediately prior to AFM probe engagement. Schillers et al. (14) overcame this obstacle with their oocyte membrane preparation by using a fluorescent marker from Molecular Probes FM1-43 that apparently fluoresces in air, eliminating the need to keep the sample moist for imaging. It could be however, that their samples were still in the process of drying, and thus not completely free of water when fluorescence imaging was done. Hydration is critical to maintain the molecular structure for fluorophore activity.
3. Additional key things learned were that typically a voltage sum above the required 0.5 V is not obtainable until fluid has been added between the fluid cell and the sample. This requires that the bottom of the fluid cell be within ~1 mm of the sample slide to allow for a meniscus to form between cell and sample. Two other potential problems with obtaining a sufficient sum are (1) not having the fluid cell squarely seated on the end of the piezo tube resulting in loss of signal into the photoarray, or (2) using a previously used tip that may have become corroded and thus less reflective. Finally, if care is not taken to do a final rinse with deionized water prior to air imaging, crystallized salts can result (Fig. 13).
4. It became clear from light microscopy, fluorescence imaging, air contact mode AFM, and fluid-tapping AFM that mitochondria are present in all SY5Y, liver, and DRG samples. From air contact mode and fluorescence imaging results, mitochondria are present in a surface area fraction between 2,000 and 10,000 per mm^2 and a volume fraction of ~0.01%, when resuspended in 10 µL. In several fluid-tapping mode images, the presence of mitochondria appears to be sparser. More than likely the scarcity is caused by rinsing to remove suspensions from the fluid-tapping arena. Resuspension in no more than 10 µL of fluid appears was sufficient to increase the

density of mitochondria to a point, where AFM is feasible with a random, nonfluorescent search. Imaging unfixed mitochondria in fluid-tapping mode is considerably more challenging because of mitochondria sticking to the probe, but is essential if in situ pore morphology is to be resolved. Timing is critical in imaging the unfixed mitochondria since osmotic swelling occurs. It does appear that imaging the full boundary of the mitochondria is significantly more challenging since the attachment to the poly-L-lysine substrate in fluid-tapping mode is much more tenuous than that in air contact mode.

5. The images obtained with this technique represent the configuration of the membrane and its proteins in situ. While it is desirable to obtain a map of where individual membrane proteins are located on the scale of seconds or fractions of a second, this is not currently feasible due to the scan rate of AFM which must necessarily be on the order of a few micrometers per second with a path width of a few nanometers. It is also unlikely that the molecular scale images attainable in planar membranes with intact proteins, e.g., (6, 33) or indeed the mitochondrial inner membrane (34) will be feasible with current AFM technology with either fixed or fresh mitochondria. However, three-dimensional reconstruction of a single cell with AFM images of serial sections has recently been achieved (35). The method described in this paper is also distinct from that used in both refs. (4) and (36), whereby immuno-labeled gold nanoparticles are used to detect the presence, prevalence, and spatial distribution of specific proteins.

Acknowledgments

The authors thank Michael Bouchard for helpful discussions on mitochondrial structure and function, Chia-Wei Wang and Hui Wang for AFM assistance, Carrie Backus and Terry Miller for mitochondrial isolation assistance, Eva Feldman for funding through the Michigan Diabetes Research and Training Center, Martin Filbert for donation of animal specimens, Ann Marie Sastry for atomic force microscope access, and the Keck Foundation for support.

References

1. Layton, B.E., et al. (2004) *In situ* imaging of mitochondrial outer membrane pores using atomic force microscopy. *BioTechniques* **37**: 564–573.
2. Feldman, E.L. (2003) Oxidative stress and diabetic neuropathy: a new understanding of an old problem. *Journal of Clinical Investigation* **111**(4): 431–3.
3. Verweij, B.H., et al. (1997) Mitochondrial dysfunction after experimental and human brain injury and its possible reversal with a selective N-type calcium channel antagonist (SNX-111). *Neurol Res* **19**(3): 334–9.
4. Papadopoulos, V., et al. (1994) Topography of the Leydig cell mitochondrial peripheral-type

benzodiazepine receptor. *Mol Cell Endocrinol* **104**(1): R5–9.

5. Goncalves, R.P., N. Buzhysnskyy, and S. Scheuring (2008) Mini review on the structure and supramolecular assembly of VDAC. *J Bioenerg Biomembr* **40**(3): 133–8.
6. Goncalves, R.P., et al. (2007) Supramolecular assembly of VDAC in native mitochondrial outer membranes. *J Mol Biol* **369**(2): 413–8.
7. Kramer, A., et al. (2008) Apoptosis leads to a degradation of vital components of active nuclear transport and a dissociation of the nuclear lamina. *Proceedings of the National Academy of Sciences of the United States of America* **105**(32): 11236–11241.
8. Joshi, N.V., et al. (2000) Ultrastructural investigation of human sperm using atomic force microscopy. *Archives of Andrology* **44**(1): 51–57.
9. Parpura, V., P.G. Haydon, and E. Henderson (1993) Three-dimensional imaging of living neurons and glia with the atomic force microscope. *J Cell Sci* **104 (Pt 2)**: 427–32.
10. Silberberg, Y.R., et al. (2008) Mitochondrial displacements in response to nanomechanical forces. *Journal of Molecular Recognition* **21**(1): 30–36.
11. Arechaga, I. and D. Fotiadis (2007) Reconstitution of mitochondrial ATP synthase into lipid bilayers for structural analysis. *Journal of Structural Biology* **160**(3): 287–294.
12. Hoogenboom, B.W., et al. (2007) The supramolecular assemblies of voltage-dependent anion channels in the native membrane. *Journal of Molecular Biology* **370**(2): 246–255.
13. Neff, D., et al. (1997) Chloroplast F0F1 ATP synthase imaged by atomic force microscopy. *Journal of Structural Biology* **119**(2): 139–148.
14. Schillers, H., et al. (2000) Plasma membrane plasticity of Xenopus laevis oocyte imaged with atomic force microscopy. *Cellular Physiology and Biochemistry* **10**(1–2): 99–107.
15. De Stasio, G., et al. (2004) Imaging the cell surface: Argon sputtering to expose inner cell structures. *Microscopy Research and Technique* **63**(2): 115–121.
16. Boujrad, N., B. Vidic, and V. Papadopoulos (1996) Acute action of choriogonadotropin on Leydig tumor cells: changes in the topography of the mitochondrial peripheral-type benzodiazepine receptor. *Endocrinology* **137**(12): 5727–30.
17. Schillers, H., et al. (2000) Plasma membrane plasticity of Xenopus laevis oocyte imaged with atomic force microscopy. *Cell Physiol Biochem* **10**(1–2): 99–107.
18. Mannella, C.A., et al. (1998) Electron microscopic tomography of rat-liver mitochondria and their interaction with the endoplasmic reticulum. *Biofactors* **8**(3–4): 225–8.
19. Handran, S.D., et al. (1997) Mitochondrial morphology and intracellular calcium homeostasis in cytochrome oxidase-deficient human fibroblasts. *Neurobiology of Disease* **3**(4): 287–298.
20. Russell, J.W., et al. (2002) High glucose-induced oxidative stress and mitochondrial dysfunction in neurons. *Faseb J* **16**(13): 1738–48.
21. Clippinger, A.J. and M.J. Bouchard (2008) Hepatitis B virus HBx protein localizes to mitochondria in primary rat hepatocytes and modulates mitochondrial membrane potential. *J Virol* **82**(14): 6798–811.
22. Clippinger, A.J., T.L. Gearhart, and M.J. Bouchard (2009) Hepatitis B virus X protein modulates apoptosis in primary rat hepatocytes by regulating both NF-kappaB and the mitochondrial permeability transition pore. *J Virol* **83**(10): 4718–31.
23. McClain, S.L., et al. (2007) Hepatitis B virus replication is associated with an HBx-dependent mitochondrion-regulated increase in cytosolic calcium levels. *J Virol* **81**(21): 12061–5.
24. Saccone, C., et al. (2003) Molecular clock and gene function. *J Mol Evol* **57 Suppl 1**: S277–85.
25. Mannella, C.A. (1998) Conformational changes in the mitochondrial channel protein, VDAC, and their functional implications. *J Struct Biol* **121**(2): 207–18.
26. Holmuhamedov, E. and J.J. Lemasters (2009) Ethanol exposure decreases mitochondrial outer membrane permeability in cultured rat hepatocytes. *Arch Biochem Biophys* **481**(2): 226–33.
27. Nitzan, Y., K. Orlovsky, and I. Pechatnikov (1999) Characterization of porins isolated from the outer membrane of Serratia liquefaciens. *Curr Microbiol* **38**(2): 71–9.
28. Kroemer, G., L. Galluzzi, and C. Brenner (2007) Mitochondrial membrane permeabilization in cell death. *Physiol Rev* **87**(1): 99–163.
29. Malin, S.A., B.M. Davis, and D.C. Molliver (2007) Production of dissociated sensory neuron cultures and considerations for their use in studying neuronal function and plasticity. *Nat Protoc* **2**(1): 152–60.
30. Schillers, H., et al. (2001) Plasma membrane protein clusters appear in CFTB-expressing Xenopus laevis oocytes after cAMP stimulation. *Journal of Membrane Biology* **180**(3): 205–212.
31. Wang, H., B.E. Layton, and A.M. Sastry (2003) Nerve collagens from diabetic and nondiabetic Sprague-Dawley and biobreeding rats: an atomic

force microscopy study. *Diabetes Metabolism Research and Reviews* **19**(4): 288–298.

32. Layton, B.E. (2008) Recent patents in bionanotechnologies: nanolithography, bionanocomposites, cell-based computing and entropy production. *Recent Patents in Nanotechnology* **2**(1): 1–12.
33. Scheuring, S., T. Boudier, and J.N. Sturgis (2007) From high-resolution AFM topographs to atomic models of supramolecular assemblies. *J Struct Biol* **159**(2): 268–76.
34. Domenech, O., et al. (2006) Thermodynamic and structural study of the main phospholipid components comprising the mitochondrial inner membrane. *Biochim Biophys Acta* **1758**(2): 213–21.
35. Chen, Y., et al. (2005) Atomic force microscopy imaging and 3-D reconstructions of serial thin sections of a single cell and its interior structures. *Ultramicroscopy* **103**(3): 173–82.
36. Layton, B.E., et al. (2008) Collagen's triglycine repeat length may help to explain an interdomain transfer event from a eukaryote into *Trichodesmium erythraeum*. *Journal of Molecular Evolution* **66**(6): 539–554.